

Relativistic quasiparticle self-consistent electronic structure of hybrid halide perovskite photovoltaic absorbers

Federico Brivio,¹ Keith T. Butler,¹ Aron Walsh,^{1, a)} and Mark van Schilfgaarde^{2, b)}

¹⁾Centre for Sustainable Chemical Technologies and Department of Chemistry, University of Bath, Claverton Down, Bath BA2 7AY, UK

²⁾Department of Physics, Kings College London, London WC2R 2LS, UK

(Dated: 3 December 2024)

Solar cells based on a light absorbing layer of the organometal halide perovskite $\text{CH}_3\text{NH}_3\text{PbI}_3$ have recently reached 15 % conversion efficiency, though how these materials work remains largely unknown. We analyse the electronic structure and optical properties within the quasiparticle self-consistent GW approximation. While this compound bears some similarity to conventional sp semiconductors, it also displays unique features. Quasiparticle self-consistency is essential for an accurate description of the band structure: bandgaps are much larger than what is predicted by the local density approximation (LDA) or GW based on the LDA. Valence band dispersions are modified in a very unusual manner. In addition, spin orbit coupling strongly modifies the band structure and gives rise to unconventional dispersion relations and a Dresselhaus splitting at the band edges. The average hole mass is small, which partially accounts for the long diffusion lengths recently observed. The surface ionisation potential (workfunction) is calculated to be 5.7 eV with respect to the vacuum level, explaining efficient carrier transfer to TiO_2 and Au electrical contacts.

One of the most promising third-generation photovoltaic technologies is based on metal-organic halide perovskites.^{1–10} The materials physics of inorganic (ABX_3) perovskites is well developed; however, the replacement of the inorganic cation by an isoelectronic organic moiety provides an opportunity for tuning the chemical bonding and optical response. We apply a range of electronic structure techniques to calculate and predict the band structure of hybrid perovskites, demonstrating how the rich and unusual physics of these materials accounts for their widely reported success as absorber layers in solar cells.

It has been established that similar to traditional dielectric perovskites, these hybrid analogues have a range of accessible polymorphs with variations in the tilting and rotation of the BX_6 polyhedra in the lattice.¹¹ A large family of hybrid perovskites have been reported with inorganic networks ranging from 1–3 dimensions.^{12–15} However, the methylammonium (MA) cation (*i.e.* CH_3NH_3^+) has been widely applied, resulting in the highest-performance perovskite-structured solar absorbers.^{2,3} The polar MA cation can also be replaced by ammonium (NH_4^+) as a smaller non-polar analogue.

Following initial studies performed using density functional theory (DFT),^{15–20} here we employ quasiparticle self-consistent GW theory²¹ (QSGW) to study the electronic structure of $\text{CH}_3\text{NH}_3\text{PbI}_3$ and NH_4PbI_3 , including the effect of spin-orbit coupling (SOC), $\lambda\mathbf{L}\cdot\mathbf{S}$, on the both the kinetic energy and electron self-energy Σ (see the Appendix). As Pb and I are heavy elements, SOC is large and has a major effect on spectral properties. SOC

predominantly modifies the kinetic energy; however, in this case relativistic effects are large enough to induce a modest reduction in Σ as well, in contrast to the vast majority of semiconductors, *e.g.* elemental Sn. As a consequence of large relativistic effects, the conduction and valence bands near the band extrema deviate strongly from parabolic behavior. Effective masses are no longer constant, but depend on doping, temperature, and the property being measured. Average effective masses are nevertheless light, and the dielectric constants large, accounting for the long diffusion lengths that have been recently reported.^{7,9}

In many respects these perovskites are similar to conventional sp semiconductors: conduction and valence bands near the Fermi level have sp character, and local-(and semi-local-) density approximation (LDA) to DFT systematically underestimate the bandgap E_G because they do not include spatial non-locality in the exchange-correlation potential. There are other significant points of departure: in sharp contrast to tetrahedral semiconductors, DFT also poorly describes valence band dispersions. This surprising result, which we discuss further below, indicates that the usual explanations invoked to account for deficiencies in DFT's description of semiconductors are not sufficient here.

We show that there is a strong feedback between dielectric response and quasiparticle levels, as occurs for CuInSe_2 ²². Thus self-consistency in GW is essential: E_G calculated from $G^{\text{LDA}}W^{\text{LDA}}$, *i.e.* LDA as the starting Hamiltonian, picks up only a little better than half the gap correction to the LDA. Moreover, the QSGW and LDA valence bands, which the LDA describes reasonably well in tetrahedral semiconductors, are significantly different. These differences underscore the limitations of density-functional based approaches (LDA, hybrid functionals, or $G^{\text{LDA}}W^{\text{LDA}}$) in describing the properties of these materials. QSGW does not depend on the LDA:

^{a)}Electronic mail:a.walsh@bath.ac.uk

^{b)}Electronic mail:mark.van_schilfgaarde@kcl.ac.uk

self-consistency renders it more reliable and universally applicable than other forms of GW , which will be important for *in silico* design of hybrid systems. Moreover, QSGW can determine some ground-state properties, e.g. the charge density and electric field gradient. Errors in QSGW tend to be small and highly systematic; most notably there is a tendency to slightly overestimate semiconductor bandgaps. Limited data is available for organic-inorganic halide perovskites, but at least for $\text{CH}_3\text{NH}_3\text{PbI}_3$ the universal tendency found in other materials is consistent with recent measurements.

Finally, based on the workfunction calculated for $\text{CH}_3\text{NH}_3\text{PbI}_3$ within DFT (including an estimate for quasiparticle corrections) we show that band alignments are consistent with efficient electron transfer to TiO_2 and Au electrical contacts.

Optimisation of the crystal structures of NH_4PbI_3 and $\text{CH}_3\text{NH}_3\text{PbI}_3$ have recently been reported¹⁹ in DFT using the PBEsol²³ exchange-correlation functional. Atomic forces were converged to within 5 meV/Å. The representative $\langle 100 \rangle$ configuration of MA is considered here. Lattice vectors of these perovskites are approximately cubic, with small distortions of the simple cubic ones. The valence band maximum and conduction band minimum falls close to a zone boundary point, the analogue of the R point $(\frac{1}{2}, \frac{1}{2}, \frac{1}{2})$ in cubic symmetry. (We denote this point as R in the remainder of the paper.)

The QP band structures for $\text{CH}_3\text{NH}_3\text{PbI}_3$, and also NH_4PbI_3 , with colours denoting the orbital character of the states, are shown in Fig. 1. The ions within the inorganic (PbI_3)⁻ cage have formal electronic configurations of Pb: $5d^{10}6s^26p^0$ and I: $5p^6$. As can be seen from the colour coding, the valence band maximum consists of approximately 70% I $5p$ and 25% Pb $6s$ (the Pb $6s$ forms a band centred around -8 eV), while the conduction band consists a mixture of Pb $6p$ and other orbitals. The molecular units CH_3NH_3 and NH_4 form σ bonds deep in the valence band. They are essentially dispersionless: they do not hybridise with the cage until energies exceed $E_F + 5$ eV. Thus their interaction with the host is largely electrostatic and structural; they provide charge compensation to the PbI_3^- cage.

The results presented in Table I demonstrate the various contributions to the band energies around the fundamental gap. The contribution from SOC (~ 1 eV), is extraordinarily large, of the order of the gap itself; so large that screening is enhanced. A smaller, but nonetheless non-negligible contribution arises from the electron self-energy ($\Sigma = iGW$), apparent from the difference between ‘SO(T)’ and ‘SO(Σ)’. Furthermore, Table I emphasises the importance of the feedback between W and QP when calculating the band structure of these systems. The ‘ GW^0 ’ gap presented, based on a perturbation of the LDA gap, are significantly smaller, due to an overestimation of the screening effect based on the LDA estimate. This is similar to situation in $\text{Cu}(\text{In},\text{Ga})\text{Se}_2$ ²², where the role of feedback is also important. The gap correction is not a simple function of the initial error in

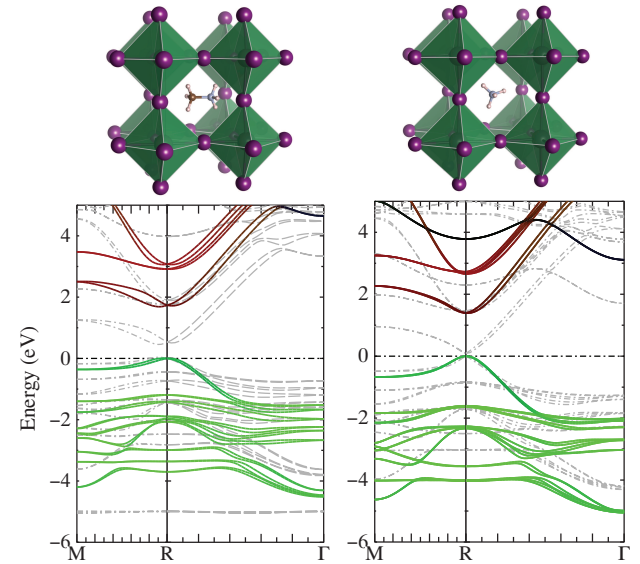


FIG. 1: QSGW band structure for $\text{CH}_3\text{NH}_3\text{PbI}_3$ (left) and NH_4PbI_3 (right). Zero denotes valence band maximum. Bands are colored according to their orbital character: green depicts I $5p$, red Pb $6p$, and blue Pb $6s$. Points denoted M and R are zone-boundary points close to $(\frac{1}{2}, \frac{1}{2}, 0)$ and $(\frac{1}{2}, \frac{1}{2}, \frac{1}{2})$, respectively. The valence band maximum (VBM) and conduction band minimum are shifted slightly from R as a consequence of the $L\cdot S$ coupling. Valence bands near -2 eV (conduction bands near +3 eV) are almost purely green (red) showing that they consist largely of I $5p$ (Pb $6p$) character. Bands nearer the gap are darker as a result of intermixing with other states. Light dashed gray lines show corresponding bands in the LDA. The dispersionless state near -5 eV corresponds to a molecular level of methylammonium. In QSGW this state is pushed down to -7.7 eV. The dispersion of the highest valence bands is very poorly described by the LDA, as described in the text.

the fundamental gap: to reliably determine the GW gap self-consistency is essential.

Recent measurements place the room temperature band gap of $\text{NH}_3\text{CH}_3\text{PbI}_3$ at 1.61 eV,²⁴ which falls slightly below the QSGW result. Some tendency for QSGW to overestimate gaps is expected. In any case theory and experiment cannot be compared to better than 0.1 eV resolution for several reasons. There are small issues with k -point convergence,²⁵ and with the shape of local wave functions determined by solving a scalar relativistic equation rather than the Dirac equation (see the Appendix); finally on the experimental side there may be some temperature dependence of the gap given the structural flexibility of the material.

Fig. 1 also shows the LDA energy bands. Remarkably, the LDA badly underestimates not only the gap but poorly describes the dispersion in the valence bands. The tendency for LDA to underestimate bandgaps is traditionally associated with the energy cost for an excited electron-hole pair. The exchange-correlation potential should distinguish between a neutral excitation (e.g. a hole shifting from one k point in the valence band to another) and one where charge is separated (excitation of

	DFT PBEsol Barth-Hedin +SO			Expt ²⁴	
NH ₃ CH ₃ PbI ₃	1.38	1.46	0.53	1.61 (RT)	
NH ₄ PbI ₃	1.20	1.13	0.09	-	
QSGW					
	SO=0	SO(T)	SO(Σ)	GW^0	Expt
NH ₃ CH ₃ PbI ₃	2.73	1.78	1.67	1.27	1.61 (RT)
NH ₄ PbI ₃	2.30	1.36	1.38	0.76	-

TABLE I: Fundamental bandgaps (in eV) of CH₃NH₃PbI₃ and NH₄PbI₃ calculated at varying levels of approximation. Top rows show DFT results using PBEsol (reported in Ref. 19) and the Barth-Hedin LDA functional. First columns show that semilocal and local functionals generate similar gaps. $\lambda\mathbf{L}\cdot\mathbf{S}$ (column '+SO') strongly reduces the gap. GW gaps are shown without SOC (SO=0), with $\lambda\mathbf{L}\cdot\mathbf{S}$ added to a fixed potential, modifying the kinetic energy only (SO(T)), and included in the QSGW self-consistency cycle (SO(Σ)). Column ' GW^0 ' is similar to SO(Σ) but G and W are generated from the LDA. (In this calculation the full Σ matrix was generated, not just the diagonal part as is customary. A Z factor of 1 was used to take partial account of self-consistency, which brings the gap in better agreement with the QSGW result; see Appendix A in Ref. 26). An error of order 0.1 eV might be associated with the treatment of SOC; see the Appendix. Room temperature (RT) band gap data is only available for NH₃CH₃PbI₃.²⁴

an electron-hole pair). Such a distinction is problematic for a local potential, which is by necessity the same for all electrons. Such an error is seen in the present case, as the LDA gap is too small. But, as Fig. 1 clearly shows, LDA and QSGW valence bands also deviate strongly from one another. Note in particular the states at R between 0 and -2 eV. This allows us to deduce that the hopping matrix elements between I 5p (and to some extent Pb 6s) states are poorly described by the LDA.

Typically light hole masses are too small in the LDA because, according to $k\cdot p$ theory, $m_v^* \propto E_G/V^2$, V being a matrix element of the gradient operator between the conduction and valence bands. m_v^* is expected to be too small because E_G is underestimated; indeed for traditional narrow gap tetrahedral semiconductors, the proportionality between m_v^* and E_G is reasonably well obeyed. The LDA predicts the light hole mass to be too small while other masses (which do not couple to the nearest conduction band) are reasonably described. For example, GaAs has a gap similar to CH₃NH₃PbI₃, and LDA underestimates it by a comparable amount (~ 1 eV). Following expectations, the LDA underestimates the light hole mass in GaAs by a factor of ~ 3 . But for CH₃NH₃PbI₃ the situation is reversed: the LDA overestimates m_v^* even while it severely underestimates E_G . For NH₄PbI₃ the LDA and QSGW masses are comparable, but only because the LDA gap is very small.

Spin-orbit coupling greatly complicates both valence and conduction bands within $k_B T$ of the band edges. We focus on the two valence bands of NH₃CH₃PbI₃, as these are the ones that govern transport in hole-based devices. As these two bands approach the R point, they must merge to the same value by symmetry. However,

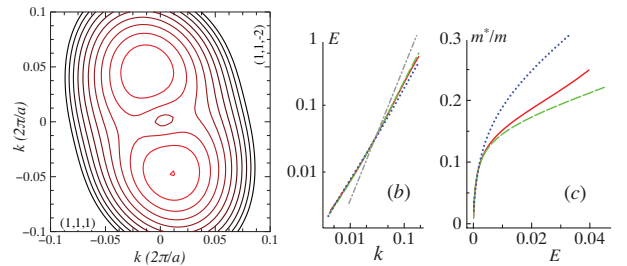


FIG. 2: Left: constant energy contours in the (1-10) plane for the upper valence band of CH₃NH₃PbI₃. The origin corresponds to the R point and [111] and [11-2] are the horizontal and vertical axes of k . Energy contours are in increments of 2.5 meV, so that the outermost contour corresponds approximately to RT. Corresponding contours in the (111) plane (not shown) appear similar. Valence bands have two maximal points near $R \pm 0.005[11\bar{2}]$. At low temperature and low doping, ($E_F < 5$ meV) the two extrema act as independent centres with approximately spherical effective masses. At high doping ($E_F > 20$ meV) or high temperature, holes effectively see a single band maximum with roughly elliptical constant energy surfaces. Panels (b) and (c) show energy $E_v(k) \equiv E(R) - E(k)$ for the lower valence band. This band has a single maximum at R , with approximately spherical dispersion. Panel (b) shows $E_v(k)$, on a log-log scale in the [110], [111], and [11-2] directions as red solid, green dashed and blue dotted lines, respectively. For comparison a parabolic band with effective mass $0.1m$ is shown as a grey dot-dashed line. Panel (c) plots $h^2 k^2 / (2m E_v)$ against E_v , which may be taken as a definition of the effective mass (see text). E_v is in eV, k in units $2\pi/a$.

they approach the R point with a linear dispersion in some directions; as a consequence the dispersions in the upper and lower bands are non-analytic. The upper band is maximum in some directions but increases with a linear slope in the $\pm[11\bar{2}]$ direction. Two maxima form near $R \pm 0.005[11\bar{2}]$ (Fig. 2(a)) arising from Dresselhaus spin-orbit coupling (which is even more pronounced in the lower conduction band). The lower band has a single maximum at R , and its constant energy surfaces deviate only modestly from spheres for k near R (Fig. 2(b)). Yet, the right panels of Fig. 2 show $E_v(k) \equiv E(R) - E(k)$ deviates markedly from a parabolic dispersion. This has important consequences for the device behavior of this material. Fig. 2(c) shows that, provided $E_v > 10$ meV, the band dispersion can be expressed approximately as a k dependent mass:

$$\frac{h^2 k^2}{2m} = m^*(k) E_v(k), \quad m^*(k) = \frac{m_0^*}{m} [1 + \alpha E_v(k)] \quad (1)$$

with $m_0^* \sim 0.12$ and α independent of $|\mathbf{k}|$ but dependent on orientation. For E_v large enough, the upper valence band can also be described by an effective mass of roughly the same size. The lower conduction band exhibits a similar behaviour, with $m_0^* \sim 0.15$. The small masses explain how these materials can exhibit high mobility and long diffusion lengths. Bands of NH₄PbI₃ differ in important details from NH₃CH₃PbI₃ (the influence of SOC is less pronounced), but the basic structure is similar. Both the bandgap and effective masses are reduced relative

to $\text{NH}_3\text{CH}_3\text{PbI}_3$, as can be seen directly by inspecting Fig. 1.

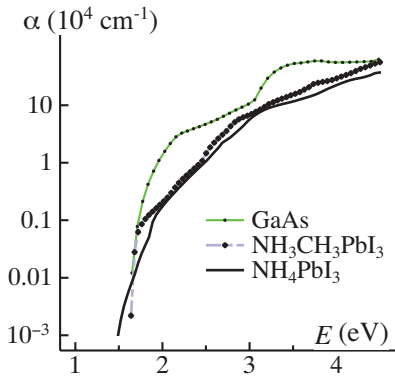


FIG. 3: Optical absorption calculated within the RPA from the QSGW potential, for $\text{CH}_3\text{NH}_3\text{PbI}_3$ and NH_4PbI_3 . The absorption is smaller than, but comparable to that of GaAs, shown for comparison. Note that similar measurements have been reported in Ref. 27.

It has been known that these compounds strongly absorb visible light. We confirm this through a random phase approximation (RPA) calculation of $\alpha(\omega)$ from the imaginary part of the macroscopic dielectric function $\epsilon_M(\omega) = [\epsilon_{\mathbf{G},\mathbf{G}'=0}^{-1}(\mathbf{q} \rightarrow 0, \omega)]^{-1}$. As Fig. 3 shows, α is somewhat smaller than – but comparable to – that of GaAs. This explains why very thin layers of the hybrid perovskites have been found to give high photovoltaic efficiencies. Indeed combined with the low carrier effective masses, the resulting electron-hole diffusion lengths exceed the typical film thickness.

	PBEsol			QSGW	
	E_G	ϵ_0	ϵ_∞	E_G	ϵ_∞
$\text{NH}_3\text{CH}_3\text{PbI}_3$	1.38	25.7	6.1	1.67	4.5
NH_4PbI_3	1.20	18.4	6.5	1.38	5.0

TABLE II: Dielectric constants (isotropic average of the tensor) and band gaps (eV), calculated in density-functional perturbation theory without SOC (from Ref. 19), and in the RPA with SOC.

Some static (ϵ_0) and high-frequency (ϵ_∞) dielectric constants are shown in Table II. These values were unusually sensitive to the k -point sampling density and require dense meshes for convergence. Those calculated by density-functional perturbation theory (e.g. PBEsol) leave out SOC and thus get fortuitously good band gaps. As a result ϵ_∞ is not so different from the QSGW case (which includes SOC). Contributions to ϵ_0 from lattice polarization are significantly larger than seen in typical tetrahedral semiconductors (compare ϵ_0 to ϵ_∞). For $\text{NH}_3\text{CH}_3\text{PbI}_3$, the value of the static dielectric constant, including quasi-particle corrections from Table II, of 24.1 is in very good agreement with permittivity measurements of 23.3.²⁸ These values exclude contributions from orientational disorder of the methylammonium ions, which will be subject to further study.²⁹

To place the electronic bands on an absolute energy scale, we have aligned the quasiparticle energies with respect to the vacuum level of a non-polar (110) termination of the perovskite, generated using *METADISE*³⁰ and using the Pb 1s core level as an energy reference. The slab model consisted of 4 perovskite layers with the dipole of the methyl ammonium cations aligned parallel to the surface termination. The resulting ionisation potential is 5.7 eV (5.9 eV from LDA, which is corrected by the GW^0 self energy), with a corresponding electron affinity of 4.0 eV. These values are in good agreement with initial photoemission measurements of thin films (5.4 eV) and explain the success of TiO_2 (electron) and Au (hole) contacts.³¹

In conclusion, we have explored the electronic structure of two key hybrid halide perovskites. Relativistic and many-body corrections are shown to be essential for a quantitative description of the materials properties important for understanding their application in photovoltaics: band gap, band dispersion, effective mass and dielectric response. These organic-inorganic materials display quantum mechanical behaviour atypical of traditional semiconductors, which begins to explain their remarkable performance in mesoporous and thin-film solar cells.

Acknowledgements. We thank L.M. Peter and H. J Snaith for useful discussions, and acknowledge membership of the UK's HPC Materials Chemistry Consortium, which is funded by EPSRC grant EP/F067496. F.B., K.T.B and A.W. are funded by the DESTINY ITN (316494), EPSRC (EP/J017361/1) and the ERC (277757), respectively.

APPENDIX: SIMPLIFIED TREATMENT OF SPIN-ORBIT COUPLING IN QSGW

Aryasetiwan and Biermann³² developed a formalism for GW with spin-dependent interactions. Rather than proceed with a completely non-collinear treatment, we take advantage of the fact that $\lambda \mathbf{L} \cdot \mathbf{S}$ is relatively small, and moreover that the non-collinear part of the eigenfunctions is unimportant for these semiconductors. We present a simplified treatment that generates results essentially as good as adding $\lambda \mathbf{L} \cdot \mathbf{S}$ non-perturbatively to the scalar Dirac Hamiltonian for M-PbI₃ compounds.

Partitioning $\mathbf{L} \cdot \mathbf{S}$ into components, the non-interacting QSGW Hamiltonian reads

$$H_0 = H_0(\lambda=0) + \lambda L^z S^z + \lambda (\mathbf{L}^+ \cdot \mathbf{S}^- + \mathbf{L}^- \cdot \mathbf{S}^+)$$

The first two terms are spin-diagonal and can be diagonalized non-perturbatively in the same manner as $H_0(\lambda=0)$. The eigenvalues ϵ_i and eigenfunctions ψ_i contain the $L^z S^z$ portion of $\mathbf{L} \cdot \mathbf{S}$, keeping ψ_i spin diagonal. The latter two terms, when treated exactly, further shift the ϵ_i and also introduce spin off-diagonal parts to the ψ_i . We allow the former but omit the latter.

The lowest order of correction to the eigenvalues is second order and we follow the spirit of second-order perturbation theory. Let δ_{ij} be the initial splitting in ϵ_i and ϵ_j , $\Delta_{ij} = |\epsilon_i - \epsilon_j|/2$. If H_{ij}^{+-} couples i and j , Δ_{ij} increases by $\delta\Delta_{ij} = |H_{ij}^{+-}|^2/|\epsilon_i - \epsilon_j|$, in lowest order.

Second-order perturbation theory can be problematic when $\epsilon_i \rightarrow \epsilon_j$. We instead obtain $\delta\Delta_{ij}$ from

$$\delta\Delta_{ij} = \sqrt{\Delta_{ij}^2 + |H_{ij}^{+-}|^2} - |\Delta_{ij}|$$

This expression is exact if i and j are isolated from the rest of the system. The final expression (the net shift for each ϵ_i is obtained by summing over each ij pair) is nevertheless correct only to second order because terms involving three or more states are not included.

We carefully tested our quasi-perturbative approach in the LDA or LDA+ U context for a wide range of materials, e.g. Fe, Sn, Au, GdN, Pu, and the perovskites addressed in this manuscript. In all cases except Pu ($Z=94$) the difference between the perturbation expression resulted in ϵ_i very close to $\mathbf{L} \cdot \mathbf{S}$ treated non-perturbatively. For $\text{CH}_3\text{NH}_3\text{PbI}_3$, for example, E_G changed by less than 0.01 eV. Self-consistency carried through with both approaches generate a slight difference in density, but no significant difference in the ϵ_i .

Tests of the adequacy of the quasi-perturbative $\mathbf{L} \cdot \mathbf{S}$ in the QSGW were performed as follows: self-consistency was reached with $\mathbf{L} \cdot \mathbf{S}$ included quasi-perturbatively, and for a given Σ , the quasiparticle levels with $\mathbf{L} \cdot \mathbf{S}$ calculated non-perturbatively were compared to the perturbative treatment. As in the LDA case, negligible differences were found for all compounds studied except for Pu, where modest differences were found. As in the LDA case, the nonperturbative treatment generated a slight change in density. Since the ϵ_i are reliably determined, it is unlikely that a better treatment of $\mathbf{L} \cdot \mathbf{S}$ (non-collinear eigenfunctions) will further affect Σ appreciably in these compounds. On the other hand, fully relativistic treatment might affect H_0 a little, since the relativistic radial functions vary as r^γ for small r , where $\gamma^2 = \kappa^2 - (2Z/c)^2$, κ playing the role of the l quantum number. γ reduces the scalar relativistic case only when $c \rightarrow \infty$. A better treatment of the small- r behavior of the partial waves modifies spin orbit splitting of the p levels for Pb by about 10%, which is not included here.

An appreciable effect of $\mathbf{L} \cdot \mathbf{S}$ on Σ is observed only for compounds with large- Z constituents. For semiconductors as heavy as Sn ($Z=50$), and for metals as heavy as Au ($Z=79$), the effect of $\mathbf{L} \cdot \mathbf{S}$ on Σ appears to be very small. But for the iodide perovskites studied here, $\mathbf{L} \cdot \mathbf{S}$ has a noticeable effect on Σ (Table I) because of the interplay between E_G and ϵ present in semiconductors but not in metals.

¹A. Kojima, K. Teshima, Y. Shirai, and T. Miyasaka, *J. Am. Chem. Soc.* **131**, 6050 (2009).

²M. M. Lee, J. Teuscher, T. Miyasaka, T. N. Murakami, and H. J. Snaith, *Science* **338**, 643 (2012).

- ³J. Burschka, N. Pellet, S.-J. Moon, R. Humphry-Baker, P. Gao, M. K. Nazeeruddin, and M. Grätzel, *Nature* **499**, 316 (2013).
- ⁴H.-S. Kim, C.-R. Lee, J.-H. Im, K.-B. Lee, T. Moehl, A. Marchioro, S.-J. Moon, R. Humphry-Baker, J.-H. Yum, and J. E. Moser, *Sci. Rep.* **2**, 591 (2012).
- ⁵J. H. Heo, S. H. Im, J. H. Noh, T. N. Mandal, C.-S. Lim, J. A. Chang, Y. H. Lee, H.-J. Kim, A. Sarkar, and M. K. Nazeeruddin, *Nature Photon.* **7**, 486 (2013).
- ⁶M. J. Carnie, C. Charbonnaeu, M. L. Davies, J. Troughton, T. M. Watson, K. Wojciechowski, H. Snaith, and D. A. Worsley, *Chem. Commun.* **49**, 7893 (2013).
- ⁷S. D. Stranks, G. E. Eperon, G. Grancini, C. Menelaou, M. J. Alcocer, T. Leijtens, L. M. Herz, A. Petrozza, and H. J. Snaith, *Science* **342**, 341 (2013).
- ⁸M. Liu, M. B. Johnston, and H. J. Snaith, *Nature* **501**, 395 (2013).
- ⁹G. Xing, N. Mathews, S. Sun, S. S. Lim, Y. M. Lam, M. Grätzel, S. Mhaisalkar, and T. C. Sum, *Science* **342**, 344 (2013).
- ¹⁰H.-S. Kim, I. Mora-Sero, V. Gonzalez-Pedro, F. Fabregat-Santiago, E. J. Juarez-Perez, N.-G. Park, and J. Bisquert, *Nature Commun.* **4** (2013).
- ¹¹T. Baikie, Y. Fang, J. M. Kadro, M. Schreyer, F. Wei, S. G. Mhaisalkar, M. Graetzel, and T. J. White, *J. Mater. Chem. A* **1**, 5628 (2013).
- ¹²J. Calabrese, N. Jones, R. Harlow, N. Herron, D. Thorn, and Y. Wang, *J. Am. Chem. Soc.* **113**, 2328 (1991).
- ¹³D. B. Mitzi, S. Wang, C. A. Feild, C. A. Chess, and A. M. Guloy, *Science* **267**, 1473 (1995).
- ¹⁴K. Liang, D. B. Mitzi, and M. T. Prikas, *Chem. Mater.* **10**, 403 (1998).
- ¹⁵I. Borriello, G. Cantele, and D. Ninno, *Phys. Rev. B* **77**, 235214 (2008).
- ¹⁶E. Mosconi, A. Amat, M. K. Nazeeruddin, M. Grätzel, and F. De Angelis, *J. Phys. Chem. C* **117**, 13902 (2013).
- ¹⁷J. Even, L. Pedesseau, J.-M. Jancu, and C. Katan, *J. Phys. Chem. Lett.* **4**, 2999 (2013).
- ¹⁸C. Quarti, G. Grancini, E. Mosconi, P. Bruno, J. M. Ball, M. M. Lee, H. J. Snaith, A. Petrozza, and F. De Angelis, *J. Phys. Chem. Lett.* **5**, 279 (2014).
- ¹⁹F. Brivio, A. B. Walker, and A. Walsh, *APL Mater.* **1**, 042111 (2013).
- ²⁰W.-J. Yin, T. Shi, and Y. Yan, *Appl. Phys. Lett.* **104**, 063903 (2014).
- ²¹M. van Schilfgaarde, T. Kotani, and S. Faleev, *Phys. Rev. Lett.* **96**, 226402 (2006).
- ²²J. Vidal, S. Botti, P. Olsson, J.-F. M. C. Guillemoles, and L. Reinig, *Phys. Rev. Lett.* **104**, 056401 (2010).
- ²³J. P. Perdew, A. Ruzsinszky, G. I. Csonka, O. A. Vydrov, G. E. Scuseria, L. A. Constantin, X. Zhou, and K. Burke, *Phys. Rev. Lett.* **100**, 136406 (2008).
- ²⁴Y. Yamada, T. Nakamura, M. Endo, A. Wakamiya, and Y. Kanemitsu, *Appl. Phys. Expr.* **7**, 032302 (2014).
- ²⁵Careful convergence checks were made of the eigenfunction and product basis. A $4 \times 4 \times 4$ k -mesh was used for the M-PbI₃ compounds. A 1-shot calculation with a $6 \times 6 \times 6$ mesh as perturbation to the QSGW result showed that the k -converged gap is about 0.1 eV larger than what is reported in Table I.
- ²⁶M. van Schilfgaarde, T. Kotani, and S. V. Faleev, *Phys. Rev. B* **74**, 245125 (2006).
- ²⁷S. De Wolf, J. Holovsky, S.-J. Moon, P. Löper, B. Niesen, M. Ledinsky, F.-J. Haug, J.-H. Yum, and C. Ballif, *J. Phys. Chem. Lett.* **In Press** (2014), 10.1021/jz500279b.
- ²⁸N. Onoda-Yamamuro, T. Matsuo, and H. Suga, *J. Phys. Chem. Sol.* **53**, 935 (1992).
- ²⁹J. M. Frost, K. T. Butler, F. Brivio, C. H. Hendon, M. van Schilfgaarde, and A. Walsh, arXiv preprint arXiv:1402.4980 (2014).
- ³⁰G. W. Watson, P. M. Oliver, and S. C. Parker, *Phys. Chem. Mater.* **25**, 70 (1997).
- ³¹N.-G. Park, *J. Phys. Chem. Lett.* **4**, 2423 (2013).
- ³²F. Aryasetiawan and S. Biermann, *Phys. Rev. Lett.* **100**, 116402 (2008).